


REPORT

TGF β -like DAF-7 acts as a systemic signal for autophagy regulation in *C. elegans*

Yujie Zhang^{1,2}, Linxiang Qi^{1,2}, and Hong Zhang^{1,2} 

In response to stress conditions, autophagy activity in multicellular organisms is systemically modulated to ensure maintenance of cellular homeostasis at an organismal level. Very little is known about the intercellular signals that elicit the long-range organism-wide autophagy response. Here we showed that during *Caenorhabditis elegans* development, loss of cuticle annular furrow collagens elicits autophagy in the hypodermis, intestine, and muscle. The cilia of sensory neurons with cuticle-localized endings are essential for triggering this systemic response. The TGF β -like molecule DAF-7, which is secreted in part from a specific pair of ciliated neurons, acts as a systemic factor that activates a canonical TGF β signaling pathway in distant tissues to induce autophagy. We also showed that AAK-2/AMPK and the STAT-like protein STA-2 act differentially in different tissues for autophagy activation. Our study reveals a circuit that senses and transduces the signal from the damaged cuticle to activate systemic autophagy during animal development.

Introduction

Autophagy involves the sequestration of cytoplasmic materials in a double-membrane autophagosome and its delivery to lysosomes for degradation (Feng et al., 2014; Mizushima et al., 2011; Zhao and Zhang, 2018). Under a variety of stress conditions, autophagy provides energy for the survival of cells. Autophagy also removes potentially toxic materials such as protein aggregates and damaged organelles to maintain cellular homeostasis.

During multicellular organism development, autophagy participates in diverse processes such as stress resistance, cell fate determination and tissue remodeling (Mizushima and Komatsu, 2011; Yang and Zhang, 2014). Studies of yeast and cultured cells have identified numerous factors that integrate various stressors with the autophagic machinery to modulate autophagy activity (Russell et al., 2014). In multicellular organisms, the stress response is coordinately controlled between different tissues/organs to ensure the maintenance of cellular homeostasis at an organismal level. Autophagy itself participates in a systemic starvation response by controlling the generation and release of cytokines, hormones, ATP, and other molecules to mediate the cross-talk between tissues/organs in energy metabolism and metabolic adaptive responses (Kaushik et al., 2011; Fenouille et al., 2017). Autophagy activity is also systemically coordinated to ameliorate deleterious effects elicited by locally imposed stresses such as nutrient restriction, and also to

maintain cell, tissue, and organism homeostasis. Up-regulation of the autophagy protein Atg1 or AMP-activated protein kinase (AMPK) in flies induces autophagy in the target tissue and also elicits a systemic autophagy response in other tissues (Ulgherait et al., 2014). Malignant tumors in fly eyes trigger autophagy in the tumor microenvironment and also in distant tissues (Katheder et al., 2017). In *Caenorhabditis elegans*, amino acids modulate the activity of the metabotropic glutamate receptor homologues MGL-1 and MGL-2 in the AIY and AIB interneurons, respectively, through a yet-to-be-identified signal to regulate systemic autophagy responses (Kang and Avery, 2009). Several signaling pathways have been identified to act non-autonomously to influence autophagy in neighboring cells or in a short-range environment. For example, the fly complement orthologue Mcr (macroglobulin complement-related) functions through the immune receptor Draper in a cell-nonautonomous manner to regulate autophagy in neighboring cells (McPhee et al., 2010; Lin et al., 2017). Systemic intercellular signaling that elicits the long-range autophagy response in distant cells/tissues/organs remain largely unknown. Glucagon and glucagon-like peptide 1 have been shown to regulate autophagy in liver and β cells (Kanasaki et al., 2019). Insulin-like peptides also modulate autophagy during animal development. In *C. elegans*, insulin-like signaling regulates entry into dauer diapause. Under harsh environmental conditions, the insulin family

¹National Laboratory of Biomacromolecules, CAS Center for Excellence in Biomacromolecules, Institute of Biophysics, Chinese Academy of Sciences, Beijing, People's Republic of China; ²College of Life Sciences, University of Chinese Academy of Sciences, Beijing, People's Republic of China.

Correspondence to Hong Zhang: hongzhang@ibp.ac.cn.

© 2019 Zhang et al. This article is distributed under the terms of an Attribution-Noncommercial-Share Alike-No Mirror Sites license for the first six months after the publication date (see <http://www.rupress.org/terms/>). After six months it is available under a Creative Commons License (Attribution-Noncommercial-Share Alike 4.0 International license, as described at <https://creativecommons.org/licenses/by-nc-sa/4.0/>).

member DAF-28 is down-regulated, accompanied by autophagy induction (Li, et al., 2003; Meléndez et al., 2003). The systemic autophagy response to tissue-specific AMPK/Atg1 induction is also associated with reduced insulin-like peptide levels in the brain (Ulgherait et al., 2014). It remains unclear whether hormones and growth factors are directly involved in systemic autophagy regulation, especially in response to environmental changes.

C. elegans is enclosed within a cuticle structure, which is essential for protection against environmental damage and pathogens, and also for body morphology and integrity. The outer layer of the cuticle contains alternating parallel circumferential bands, known as annuli and annular furrows, which comprise two discrete interacting groups of collagens (McMahon et al., 2003). Loss of function of annular furrow collagen genes, including *dpy-2*, *-7*, and *-10*, manifests as cuticle damage and elicits innate immune response and osmotic resistance phenotypes (Lamitina et al., 2006; Wheeler and Thomas, 2006; Pujol et al., 2008a,b). Here we demonstrated that loss of annular furrow collagens triggers systemic induction of autophagy. The cilia of sensory neurons, whose endings are embedded in the subcuticle or exposed to the external environment via openings in the cuticle (Inglis et al., 2007), are required for autophagy induction. The TGF β molecule DAF-7, which is secreted from ciliated neurons, acts as a systemic factor to activate autophagy in distal cells. Our study revealed a circuit for sensing and coordinating autophagy regulation in different tissues in response to cuticle damage during worm development.

Results and discussion

Loss of function of the cuticle annular furrow-related collagen genes promotes autophagy activity

During *C. elegans* development, EPG-7 acts as a scaffold protein to facilitate autophagic degradation of the p62 homologue SQST-1 (Fig. 1, A, A', B, and H; Tian et al., 2010; Lin et al., 2013). We performed genetic screens and identified a mutation, *bp1237*, that caused a dramatic reduction in the number of SQST-1::GFP aggregates in *epg-7* mutants (Fig. 1, C and H). Simultaneous depletion of *lgg-1* restored the accumulation of SQST-1 aggregates in *epg-7*; *bp1237* mutants (Fig. 1, D and H). Levels of SQST-1::GFP protein were also decreased in *epg-7*; *bp1237* mutants (Figs. 1I and S1 U), while *sqst-1* mRNA levels remained unchanged (Fig. S1 A). *bp1237* exhibited a shorter and stout dumpy phenotype, known as *Dpy*, that is similar to animals lacking cuticle collagen genes (Fig. S1, B and C). Genetic mapping and transformation rescue experiments demonstrated that *bp1237* is an allele of *dpy-10* (Fig. 1, E and H; and Fig. S1, D and E). Accumulation of SQST-1::GFP aggregates in *atg-18(bp594)* hypomorphic mutants and in *rpl-43(bp399)* mutants, but not in null mutants of autophagy genes required for autophagosome formation, was also suppressed by loss of *dpy-10* activity (Fig. 1, F-H; and Fig. S1, F-I, N, and O).

The level of the lipidated *C. elegans* Atg8 homologue LGG-1 (LGG-1-II) has been widely used to monitor autophagy activity (Zhang et al., 2015a). In *dpy-10* mutants, both LGG-1-I (unlipidated) and LGG-1-II levels were reduced (Figs. 1 J and S1 V), which could be explained by elevated autophagy activity or

impaired autophagy at the induction step. To distinguish between these two possibilities, we determined the levels of LGG-1 in *epg-5 dpy-10* double mutants. In *epg-5* mutants, non-degradative autolysosomes accumulate, resulting in accumulation of LGG-1 puncta and elevated levels of LGG-1-II (Fig. 1, K, L, N, and O; and Fig. S1 W; Tian et al., 2010). Accumulation of LGG-1 puncta in *epg-5* mutants is ameliorated by a block in autophagy induction and aggravated by an elevation of autophagy induction (Guo et al., 2014; Wang et al., 2016). The number of GFP::LGG-1 puncta and levels of LGG-1-II in *epg-5* mutants were greatly enhanced by simultaneous loss of *dpy-10* (Fig. 1, M-O; and Fig. S1 W). mRNA levels of six autophagy genes analyzed were not up-regulated in *dpy-10* mutants (Fig. S1 Q). These results indicate that loss of *dpy-10* activity elevates autophagy activity.

According to their function in the formation of annular furrows, *Dpy* genes are classified into two groups (McMahon et al., 2003). Annuli are absent in mutants of *dpy-10* family genes (i.e., *dpy-2*, *dpy-3*, *dpy-7*, *dpy-8*, and *dpy-10*), but not in mutants of *dpy-13* family genes (i.e., *dpy-5* and *dpy-13*; McMahon et al., 2003; Page and Johnstone, 2007). An allele of *dpy-2*, *bp1242*, was also isolated in the aforementioned screen (Fig. S1, J-K and P). Loss of function of other *dpy-10* family genes, but not *dpy-5*, suppressed accumulation of SQST-1::GFP aggregates in *epg-7* mutants (Fig. S1, L-M' and P).

Loss of function of *dpy-10* results in systemic autophagy activation

We characterized autophagy activity in tissues that are in direct contact with or separate from the cuticle. To facilitate the analysis, transgenes expressing SQST-1::GFP in specific tissues were used, including hypodermal cells (*bpIs267*; Fig. 2, A, B, and B'), intestinal cells (*bpIs262*; Fig. 2, A, E, and E'), and body wall muscles (*bpIs287*; Fig. 2, A, H, and H'). SQST-1::GFP aggregates accumulated in *epg-7* mutants carrying *bpIs267* or *bpIs262* (Fig. 2, C, F, J, K, M, and N; and Fig. S1, X and Y), and this accumulation was dramatically reduced by simultaneous loss of function of *dpy-10*, but not *dpy-5* (Fig. 2, D, G, J, K, M, and N; and Fig. S1, R, S, X, Y, and A1-B1'). Animals carrying *bpIs287* accumulated SQST-1::GFP aggregates in muscle cells (Fig. 2, H, H', L, and O; and Fig. S1 Z), and this phenotype was further enhanced in *epg-7* mutants (Fig. S1, D1 and D1'). *dpy-10(bp1237)*, but not *dpy-5*, suppressed accumulation of SQST-1::GFP aggregates in *bpIs287* and also in *epg-7*; *bpIs287* animals (Fig. 2, I, L, and O; and Fig. S1, T, Z, C1-E1, and J1). Accumulation of SQST-1::GFP aggregates in the hypodermis and intestine in *epg-5* mutants failed to be suppressed by *dpy-10* inactivation (Fig. S1, F1-I1, K1, and L1). Thus, autophagic activity is activated in multiple tissues by inactivation of annular furrow-related collagen genes.

Cilia are essential for systemic autophagy activation in *dpy-10* mutants

In *C. elegans*, the cilia of sensory neurons are involved in sensing the chemical and physical extracellular environments in *C. elegans* (Inglis et al., 2007). The formation and function of cilia depends on continuous trafficking of structural, regulatory, and signaling molecules by intraflagellar transport (IFT), which is

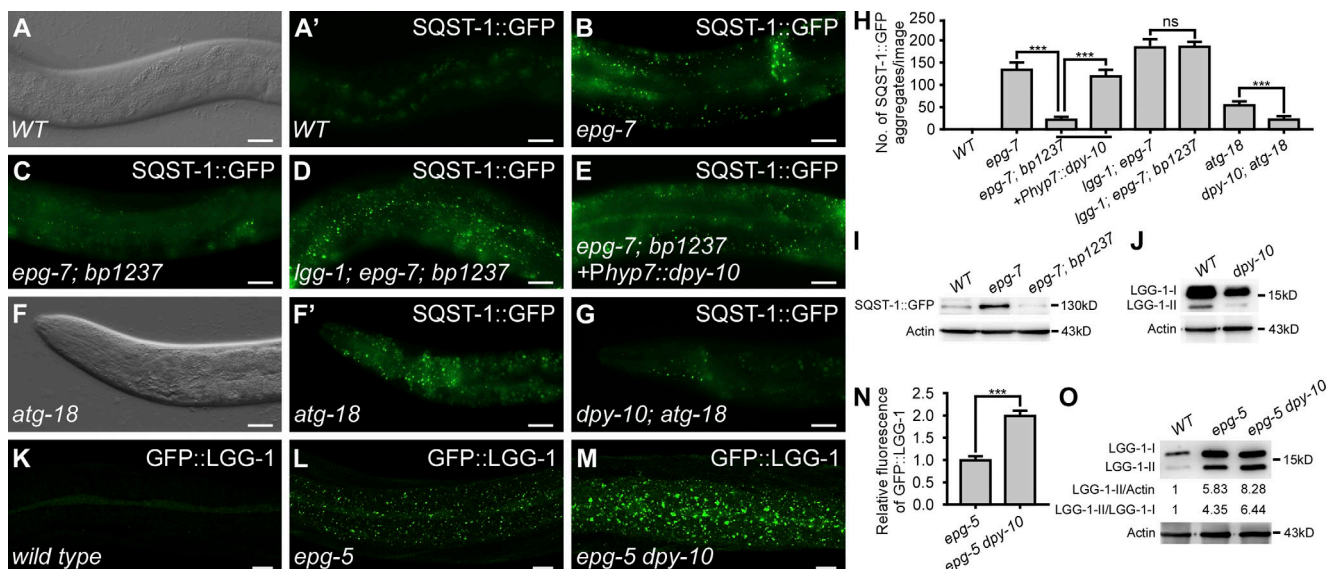


Figure 1. Loss of function of *dpy-10* promotes autophagy activity. (A and A') Weak SQST-1::GFP signal is diffusely localized in wild-type larvae. (A) Differential interference contrast (DIC) image of the animal in A'. The irregular fluorescence signals in the intestine are gut autofluorescence. (B and C) Accumulation of SQST-1::GFP aggregates in *epg-7* mutants (B) is suppressed by *bp1237* (C). (D and E) Accumulation of SQST-1 aggregates in *epg-7; bp1237* mutants is restored by *lgg-1(RNAi)* (D), and also by a transgene expressing *dpy-10* genomic DNA (E). The transgenic line *bpls151(Psqst-1::sqst-1::gfp)*, in which *sqst-1* is driven by its own promoter, is used in A–E. Late L4 larvae are shown in A–E. (F and G) *dpy-10(RNAi)* suppresses accumulation of SQST-1::GFP aggregates in *atg-18(bp594)* mutants. (F) DIC image of the animal in F'. (H) The number of SQST-1::GFP aggregates in the indicated strains. Five independent images of the same body region in five animals ($n = 5$) for each strain were quantified. Data are shown as mean \pm SEM in this study; ns, no significant difference; ***, $P < 0.001$. (I) Levels of SQST-1::GFP in extracts of animals with the indicated genotype. (J) Levels of LGG-1-I (unlipidated) and LGG-1-II (lipidated form) in wild-type and *dpy-10(bp1237)* mutant animals. (K) Weak GFP::LGG-1 signal is diffusely localized in wild-type larvae. (L–N) GFP::LGG-1 puncta accumulate in the hypodermis in *epg-5(tm3425)* mutants (L), and this accumulation is further enhanced by *dpy-10(RNAi)* (M). (N) Quantification of relative fluorescence intensity of GFP::LGG-1 ($n = 6$). Data are shown as mean \pm SEM; ***, $P < 0.001$. (O) Levels of LGG-1-II and the ratio of LGG-1-II/LGG-1-I in the indicated strains. The level or ratio in wild-type animals is set to 1.0. Scale bars: A–G, 20 μ m; K–M, 10 μ m.

mediated by a multiprotein complex. The cilia of amphid and phasmid neurons, labeled with a reporter for the IFT protein OSM-6, were normal in *dpy-10* mutants (Fig. S2, A–D). Loss of function of *che-3*, which encodes a dynein heavy chain 1b isoform involved in retrograde IFT, caused no defect in degradation of SQST-1 and did not affect accumulation of SQST-1 aggregates in *epg-7* mutants (Fig. 3, A, B, E, F, I, and I'). Loss of *che-3* activity restored the accumulation of SQST-1::GFP aggregates in hypodermal and intestinal cells in *dpy-10; epg-7* mutants (Fig. 3, C, G, L, and M). SQST-1::GFP aggregates also persisted in the muscle in *che-3; dpy-10* mutants (Fig. 3, J and N). Loss of function of *osm-3*, which encodes the IFT motor kinesin-II homologue, also abolished the suppressing effect of *dpy-10(bp1237)* (Fig. S2, E–M). These results suggest that cilia are involved in sensing the cuticle damage and activating autophagy in distal tissues in *dpy-10* mutants.

The TGF β molecule DAF-7 is required for systemic autophagy activation in *dpy-10* mutants

We next sought the signal that is transduced from ciliated neurons to trigger the long-range autophagy response. Loss of function of genes involved in synaptic transmission or in generation and release of neuropeptides, including *unc-13*, *unc-31*, *egl-3*, and *egl-21* (Richmond et al., 1999; Li and Kim, 2008), had no effect on the suppressing effect of *dpy-10* inactivation (Fig. S2, N–K1). In response to changes in environmental conditions,

ciliated sensory neurons secrete DAF-7, a TGF β -related ligand for the dauer TGF β pathway. Once secreted, DAF-7 activates a canonical TGF β signaling pathway in target tissues (Fig. 3 O; Hu, 2007). Loss of function of *daf-7* had no effect on SQST-1::GFP removal and did not affect the defective degradation of SQST-1 in *epg-7* mutants (Fig. 3, P, Q, X, Y, D1, and D1'). We found that loss of *daf-7* activity restored the accumulation of SQST-1::GFP aggregates in the hypodermis and intestine of *dpy-10; epg-7* mutants (Fig. 3, R, Z, I1, and J1) and in the muscle of *dpy-10* mutants (Fig. 3, E1 and K1). The receptor encoding gene *daf-1* was also required for the suppressing effect of *dpy-10* inactivation (Fig. S3, A–I). In contrast, simultaneous depletion of the antagonistic coSMAD DAF-3 suppressed the accumulation of SQST-1::GFP aggregates in the hypodermis and intestine in *dpy-10; daf-7; epg-7* mutants and in the muscle in *dpy-10; daf-7* mutants (Fig. 3, T, B1, G1, and I1–K1). Thus, dauer TGF β signaling is required for systemic autophagy activation in *dpy-10* mutants.

Expression of *daf-7* is mainly limited to the ASI pair of ciliated neurons, and the *daf-7* expression level in these cells is modulated by the availability of food and pheromones, and also by infection (Fig. 3 L1; Hu, 2007; Meisel et al., 2014). The *Pgpa-4::daf-7* transgene, in which *daf-7* is specifically expressed in the ASI neurons, was sufficient to rescue the effect of *daf-7(ok3125)* on SQST-1::GFP aggregate accumulation in *dpy-10; daf-7; epg-7* mutants as well as in *dpy-10; daf-7* mutants (Fig. 3, S, A1, F1, and I1–K1). The fluorescence signal of a *Pdaf-7::gfp*

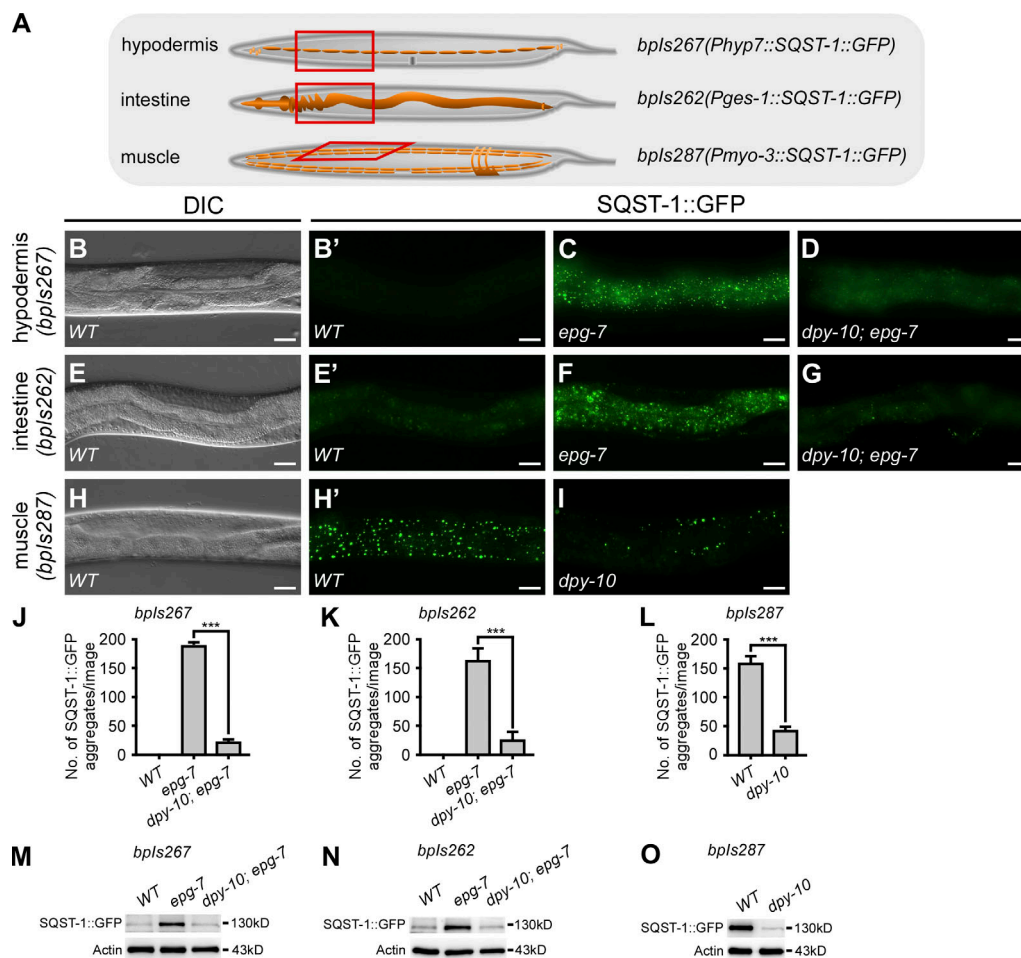


Figure 2. Loss of function of *dpy-10* causes systemic autophagy activation. (A) Schematic illustration of tissue-specific expression of SQST-1::GFP. Each tissue is highlighted in orange. The red box indicates the region used for analysis. The corresponding reporters are also listed. (B and B') Weak SQST-1::GFP signal is diffusely localized in animals carrying *bpls267*. (C and D) Accumulation of SQST-1::GFP aggregates in the hypodermis in *epg-7* mutants (C) is suppressed by *dpy-10*(*bp1237*) (D). (E and E') SQST-1::GFP is weakly expressed in the intestine in wild-type animals carrying *bpls262*. The irregular fluorescence signals are gut autofluorescence. (F and G) SQST-1::GFP aggregates accumulate in the intestine in *epg-7* mutants (F), and this accumulation is suppressed in *dpy-10*(*bp1237*); *epg-7* double mutants (G). (H and I) SQST-1::GFP forms a large number of aggregates in the muscle in wild-type animals carrying *bpls287* (H'), while the number of aggregates is much lower in *dpy-10* mutants (I). (B, E, and H) DIC images of the animals in B', E', and H', respectively. (J-L) Quantification of the number of SQST-1::GFP aggregates in the indicated strains ($n = 5$ for each strain). Data are shown as mean \pm SEM; ***, $P < 0.001$. (M-O) Levels of SQST-1::GFP in extracts of the indicated strains. Scale bars: 20 μ m.

transcriptional reporter was stronger in ASI neurons in *dpy-10* mutants than in wild-type animals (Fig. 3, M1-O1). Expression of *daf-3* specifically in the ASI neurons or in the muscle, however, failed to rescue the phenotype in the hypodermis in *dpy-10*; *daf-7*; *daf-3*; *epg-7* mutants (Fig. 3, V, W, and I1). Accumulation of SQST-1::GFP aggregates in the hypodermis and intestine in *dpy-10*; *daf-7*; *daf-3* *epg-7* mutants and in the muscle of *dpy-10*; *daf-7*; *daf-3* mutants was restored by expression of *daf-3* driven by hypodermis-, intestine-, and muscle-specific promoters, respectively (Fig. 3, U, C1, and H1-K1). These results indicate that DAF-3 functions cell-autonomously in regulating autophagy in *dpy-10* mutants. Simultaneous depletion of *dpy-10* suppressed accumulation of SQST-1::GFP aggregates in the hypodermis and intestine in *che-3*; *daf-3*; *epg-7* triple mutants and in the muscle in *che-3*; *dpy-10*; *daf-3* mutants (Fig. 3, D, H, and K-N). Thus, TGF β signaling acts downstream of cilia in activating autophagy in distal tissues in *dpy-10* mutants.

AAK-2/AMPK and STA-2 act differentially in different tissues to activate autophagy in *dpy-10* mutants

We examined the role of the *C. elegans* AMPK catalytic subunit (AMPK α) orthologue, AAK-2, in autophagy activation in *dpy-10* mutants. The expression of the functional AAK-2 reporter, AAK-2(aal-321)::Tomato, was increased in *dpy-10* mutants compared with control animals (Fig. 4, A-C). Phosphorylation of Thr172 in the activation loop of human AMPK α is required for AMPK activation, and the residues surrounding the phosphorylated Thr residue are conserved in AAK-2 (Mihaylova and Shaw, 2011). In *dpy-10* mutants, levels of phosphorylated AAK-2, detected by the antibody recognizing Thr172-phosphorylated AMPK, were increased (Figs. 4 D and S3 J). Loss of function of *aak-2* had no effect on SQST-1::GFP removal and did not affect SQST-1::GFP accumulation in *epg-7* mutants (Fig. 4, E and F; and Fig. S3, K, K', M, and M'). SQST-1::GFP aggregates accumulated in the hypodermis in *dpy-10*; *epg-7*; *aak-2* mutants (Fig. 4, G and U).

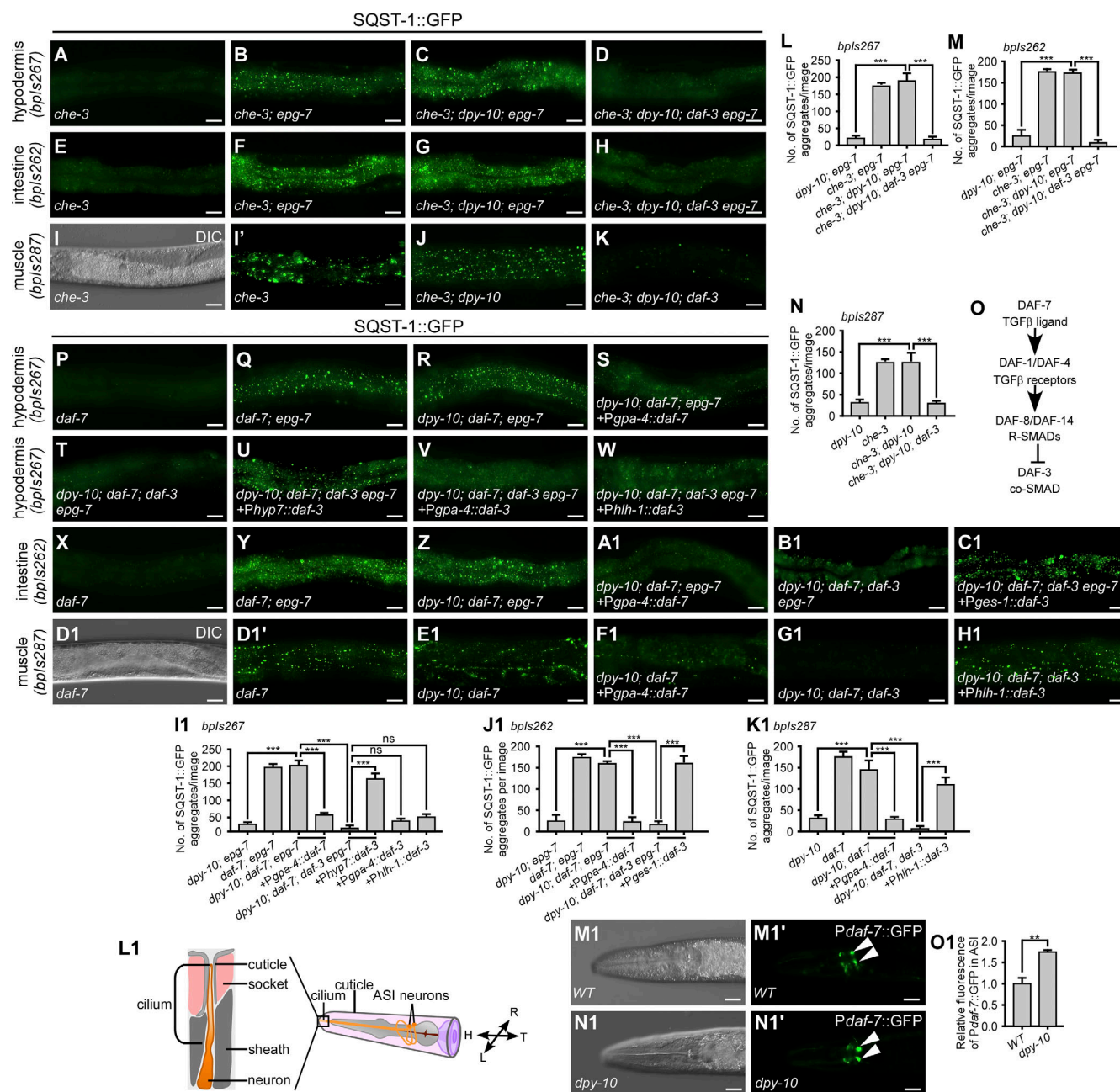


Figure 3. Functional cilia and TGFβ signaling are essential for systemic autophagy activation in *dpy-10* mutants. (A and E) Weak SQST-1::GFP signal is diffusely localized in the hypodermis (A) and intestine (E) in *che-3* mutants. (B, C, F, and G) SQST-1::GFP aggregates accumulate in *che-3; epg-7* mutants (B and F); this accumulation is not suppressed by *dpy-10* inactivation (C and G). (D and H) Accumulation of SQST-1::GFP aggregates in *che-3; dpy-10; epg-7* mutants in the hypodermis (D) and intestine (H) is suppressed by *daf-3* inactivation. (I and J) SQST-1::GFP aggregates accumulate in the muscle in *che-3* mutants (I') and also in *che-3; dpy-10* mutants (J). (I) DIC image of the animal shown in I'. (K) Accumulation of SQST-1::GFP aggregates in the muscle in *che-3; dpy-10* mutants is suppressed by *daf-3* inactivation. (L–N) Quantification of the number of SQST-1::GFP aggregates in the indicated strains ($n = 5$ for each strain). Data are shown as mean \pm SEM; ***, $P < 0.001$. (O) Diagram of components in the dauer TGFβ signaling pathway. (P) Weak diffuse SQST-1::GFP is detected in the hypodermis in *daf-7* mutants. (Q and R) SQST-1::GFP aggregates accumulate in the hypodermis in *daf-7; epg-7* mutants (Q). Depletion of *dpy-10* fails to suppress this phenotype (R). (S and T) Accumulation of SQST-1::GFP aggregates in the hypodermis in *dpy-10; daf-7; epg-7* mutants is suppressed by expressing the *Pgpa-4::daf-3* transgene (S), and also by depletion of *daf-3* (T). (U–W) Accumulation of SQST-1::GFP aggregates in the hypodermis in *daf-7; daf-3 epg-7* mutants is restored by expressing *daf-3* in the hypodermis (U), but not in the ASI neurons (V) or the muscle (W). (X–Z) Weak SQST-1::GFP is diffusely localized in the intestine in *daf-7* mutants (X), while a large number of SQST-1::GFP aggregates accumulate in *daf-7; epg-7* mutants (Y) and *dpy-10; daf-7; epg-7* (Z) mutants. (A1 and B1) Accumulation of SQST-1::GFP aggregates in the intestine in *dpy-10; daf-7; epg-7* mutants is suppressed by the *Pgpa-4::daf-7* transgene (A1) or by depletion of *daf-3* (B1). (C1) Accumulation of SQST-1::GFP aggregates in the intestine in *dpy-10; daf-7; daf-3 epg-7* mutants is restored by *Pges-1::daf-3*. (D1 and E1) As in wild-type animals, a large number of SQST-1::GFP aggregates accumulate in the muscle in *daf-7* mutants carrying *bpls287* (D1'). Inactivation of *dpy-10* fails to suppress this phenotype (E1). (D1') DIC image of the animal in D1'. (F1 and G1) Expression of the *Pgpa-4::daf-7* transgene (F1) or depletion of *daf-3* (G1) suppresses accumulation of SQST-1::GFP aggregates in the muscle in *dpy-10; daf-7* mutants. (H1) Expression of *daf-3* driven by the muscle-specific *hlh-1* promoter (H1) restores accumulation of SQST-1::GFP aggregates in the muscle in *dpy-10; daf-7; daf-3* mutants. (I1–K1) Quantification of the number of

SQST-1::GFP aggregates in the indicated strains carrying the indicated transgene ($n = 5$ for each strain). Data are shown as mean \pm SEM; ***, $P < 0.001$. (L1) Left: Schematic illustration of the ciliated ending of the ASI neuron. ASI is one of 11 amphid neurons associated with the pores in the cuticle, which are generated by amphid socket cells. Right: Positions of the ASI ciliated cell bodies and their dendritic extensions. Images are adapted from Perkins et al. (1986). (M1–O1) Compared with wild-type animals, the fluorescence intensity of *Pdaf-7::gfp* in the ASI pair of neurons is increased in *dpy-10* mutants (N1'). (M1 and N1) DIC images of the animals in M1' and N1', respectively. Quantification of the fluorescence intensity is shown in O1 ($n = 5$). Data are shown as mean \pm SEM; **, $P < 0.01$. Scale bars: 20 μ m.

Expression of AAK-2 specifically in the hypodermis rescued this effect of *aak-2* inactivation, suggesting that AAK-2 acts cell-autonomously to activate autophagy (Fig. 4, H and U). In *dpy-10*; *daf-3* *epg-7* *aak-2* mutants, SQST-1::GFP aggregates accumulated in the hypodermis (Fig. 4, I and U), indicating that AAK-2 functions downstream of or in parallel to TGF β signaling. SQST-1::GFP aggregates were still absent in the intestine of *dpy-10*; *epg-7* *aak-2* mutants and in the muscle of *dpy-10*; *aak-2* mutants (Fig. S3, L, N, U, and V). Thus, AAK-2 is required for elevated autophagy activity in the hypodermis, but is dispensable in the intestine and muscle of *dpy-10* mutants.

PMK-1 p38 MAPK signaling and the STAT-like protein STA-2 are involved in triggering the innate immune response in the hypodermis and intestine in response to environmental stresses (Pujol et al., 2008a,b; Dierking et al., 2011; Zhang et al., 2015b). Loss of function of *pmk-1* and *sta-2* had no effect on degradation of SQST-1 aggregates (Fig. 4, J, J', K, N, N', O, R, and R'; and Fig. S3, O, O', Q, Q', S, and S'). Loss of *dpy-10* activity suppressed accumulation of SQST-1::GFP aggregates in the hypodermis in *pmk-1*; *epg-7* mutants and *sta-2*; *epg-7* mutants (Fig. S3, P, T, and W). In the intestine of *dpy-10*; *epg-7* mutants, accumulation of SQST-1::GFP aggregates was restored by loss of activity of *pmk-1* or *sta-2* (Fig. 4, L, P, V, and W). Simultaneous *daf-3* inactivation suppressed the accumulation of SQST-1::GFP aggregates in the intestine in *dpy-10*; *pmk-1*; *epg-7* mutants and *dpy-10*; *sta-2*; *epg-7* mutants (Fig. 4, M, Q, V, and W), suggesting that PMK-1 and STA-2 function upstream of or in parallel to DAF-3 in regulating autophagy in *dpy-10* mutants. Accumulation of SQST-1::GFP aggregates was suppressed in muscle cells in *dpy-10*; *pmk-1* mutants (Fig. S3, Q, Q', R, and V). SQST-1::GFP aggregates persisted in the muscle in *dpy-10*; *sta-2* mutants but were absent in *dpy-10*; *sta-2*; *daf-3* mutants (Fig. 4, S, T, and X). Therefore, in *dpy-10* mutants, PMK-1 is dispensable for autophagy activation in the hypodermis and muscle, while STA-2 is dispensable in the hypodermis but required in the intestine and muscle.

The elevated innate immunity and osmotic stress resistance in *dpy-10* mutants are independent of autophagy activation

Loss of function of *dpy-10* family members triggers the innate immune response, as shown by up-regulation of neuropeptide-like proteins, and also elevates expression of hyperosmotic stress response genes, such as *gpdh-1*, which encodes glycerol-3-phosphate dehydrogenase (Lamitina et al., 2006; Wheeler and Thomas, 2006; Pujol et al., 2008b). Loss of activity of *osm-7*, which activates the osmosensitive response, failed to suppress the accumulation of SQST-1::GFP aggregates in *epg-7* mutants (Fig. S3, X–Y'). Up-regulation of *Pnlp-29::GFP* and *Pgpdh-1::GFP* in *dpy-10* mutants remained unaffected by simultaneous depletion of *che-3*, *daf-7*, or *aak-2* (Fig. S3, Z–N1). Therefore, functional

cilia, dauer TGF β signaling, and AMPK/AAK-2 are not involved in the innate immune response and hypertonic stress in *dpy-10* mutants.

Here we revealed a circuit that senses and transduces the cuticle damage caused by loss of function of the cuticle annular furrow collagen genes to trigger systemic induction of autophagy (Fig. 4 Y). The nature of the signal in *dpy-10* family gene mutants that is perceived by the ciliated sensory neurons has yet to be determined. DAF-7 secreted from the ASI pair of ciliated neurons acts as a systemic factor to activate a canonical TGF β signaling pathway in distant tissues to activate autophagy in *dpy-10* mutants. Different signaling pathways are involved in triggering expression of distinct stress response genes caused by the cuticle damage in annular furrow-related collagen gene mutants (Pujol et al., 2008a,b). Our study sheds new light on the systemic signals that elicit long-range autophagy responses to environmental stress for maintaining cell, tissue, and organism homeostasis.

Materials and methods

Worm strains

The following strains were used in this work: *aak-2(ok524)*, *atg-18(bp594)*, *che-3(cas495)*, *daf-1(m40)*, *daf-3(tm4698)*, *daf-7(ok3125)*, *dpy-2(bp1242)*, *dpy-5(e61)*, *dpy-10(bp1237)*, *dpy-10(e128)*, *egl-3(nr2090)*, *egl-21(n476)*, *epg-5(tm3425)*, *epg-7(tm2508)*, *osm-3(p802)*, *pmk-1(km25)*, *rpl-43(bp399)*, *sta-2(ok1860)*, *unc-13(e1091)*, *unc-31(e169)*, *bpIs151(Psqst-1::sqst-1::GFP+unc-76)*, *bpIs267(Phyph7::sqst-1::gfp+unc-76)*, *bpIs262(Pges-1::sqst-1::gfp+unc-76)*, *bpIs287(Pmyo-3::sqst-1::gfp+unc-76)*, *bpIs360(Prgef-1::sqst-1::gfp+Pord-1::rfp)*, *bpIs345(Pgpdh-1::gfp+unc-76)*, *adIs2122(lgg-1p::GFP::lgg-1+rol-6(su1006))*, *mnIs17(osm-6p::osm-6::gfp+unc-36)*, *uthIs202(aak-2(intron 1)::aak-2(aal-aa321)::Tomato::unc-54 3'UTR+rol-6(su1006))*, and *frIs7(nlp-29p::GFP+col-12p::dsRed)*.

Mapping and cloning of *dpy-2* and *dpy-10*

epg-7 mutants carrying the *bpIs151* transgene were used for ethyl methanesulfonate mutagenesis. *bp1237* and *bp1242* were isolated from a screen of ~5,000 genomes for mutations that dramatically decreased the number of SQST-1::GFP aggregates compared with *epg-7* single mutants. Both *bp1237* and *bp1242* were mapped to chromosome II by single nucleotide polymorphism mapping. A transgene containing fosmid WRM0636aD09 restored the accumulation of SQST-1::GFP in *epg-7*; *bp1237* or *epg-7*; *bp1242* mutants. *bp1237* and *bp1242* cause a Dpy phenotype. *dpy-10* and *dpy-2* are located in the region where *bp1237* and *bp1242* are mapped. A transgene expressing *dpy-10* and *dpy-2* rescued the phenotype in *bp1237* and *bp1242* mutants, respectively. The molecular lesions in *bp1237* and *bp1242* were determined by sequencing. *bp1237* contains a deletion that removes 163 amino

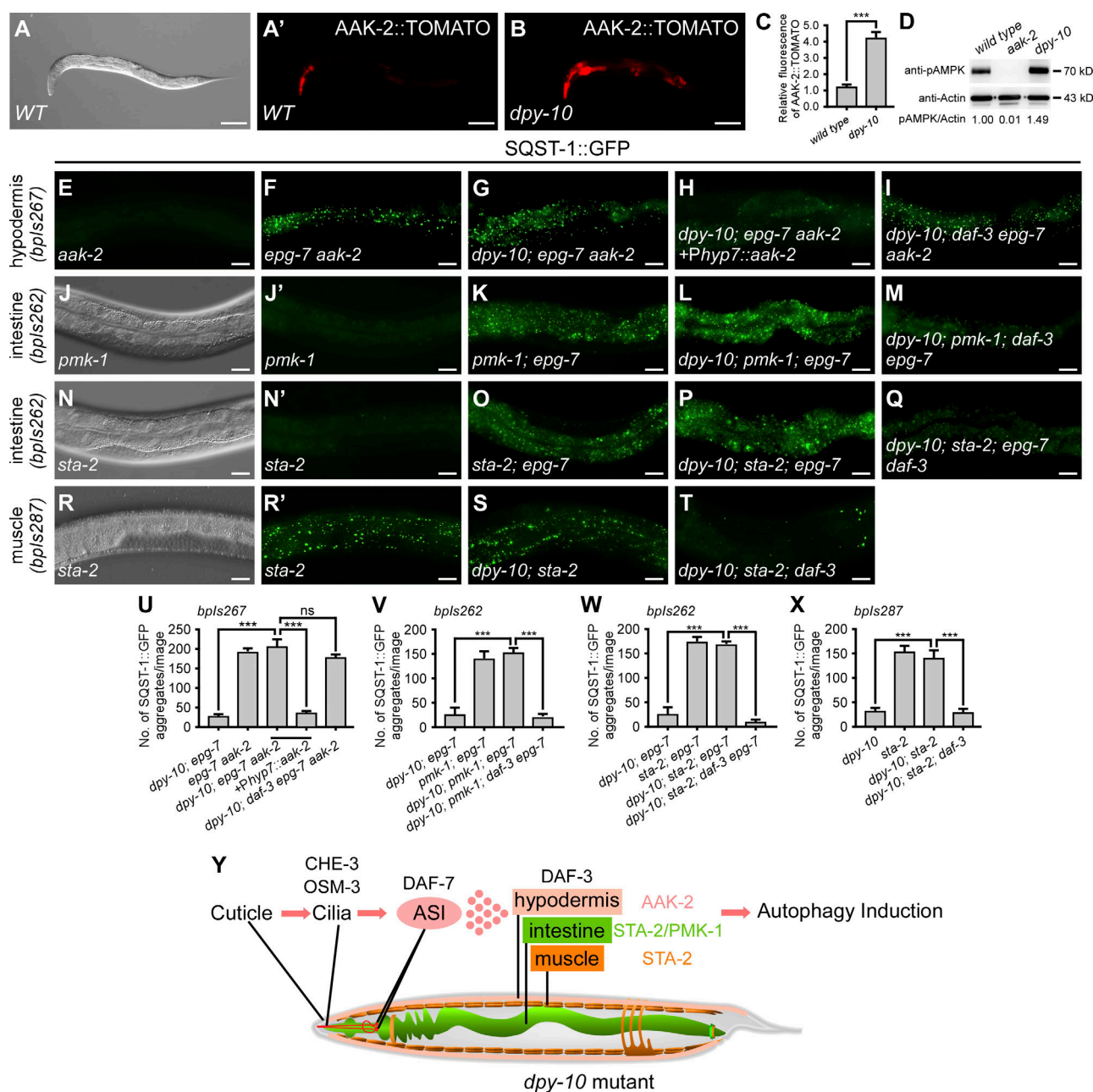


Figure 4. AAK-2, PMK-1, and STA-2 act differentially in different tissues to activate autophagy in *dpy-10* mutants. (A–C) Compared with wild-type animals (A'), the fluorescence intensity of AAK-2(aal-321)::Tomato is increased in *dpy-10* mutants (B). (C) Quantification of relative fluorescence intensity ($n = 10$ for each strain). Data are shown as mean \pm SEM; ***, $P < 0.001$. (D) Level of phosphorylated AMPK in wild-type and *dpy-10* mutant extracts. The absence of signal in *aak-2* mutant extracts confirms the antibody specificity. The level of pAMPK in wild-type animals (normalized by actin levels) is set to 1.00. (E) Weak SQST-1::GFP signal is diffusely localized in *aak-2(ok524)* mutants. (F and G) SQST-1::GFP aggregates accumulate in the hypodermis in *epg-7 aak-2* mutants (F). Depletion of *dpy-10* fails to suppress this phenotype (G). (H) Accumulation of SQST-1::GFP aggregates in *dpy-10; epg-7 aak-2* mutants is suppressed by the *Phyp7::aak-2* transgene. (I) SQST-1::GFP aggregates accumulate in *dpy-10; daf-3 epg-7 aak-2* mutants. (J and J') Weak diffuse SQST-1::GFP signal is detected in the intestine in *pmk-1(km25)* mutants. (K and L) SQST-1::GFP aggregates accumulate in the intestine in *pmk-1; epg-7* mutants (K). Inactivation of *dpy-10* fails to suppress this phenotype (L). (M) Depletion of *daf-3* suppresses accumulation of SQST-1::GFP aggregates in *dpy-10; pmk-1; epg-7* mutants. (N–P) Compared with *sta-2(ok1860)* mutants (N'), SQST-1::GFP aggregates accumulate in the intestine in *sta-2; epg-7* mutants (O). This accumulation is not suppressed by simultaneous depletion of *dpy-10* (P). (Q) Loss of function of *daf-3* suppresses the accumulation of SQST-1::GFP aggregates in *dpy-10; sta-2; epg-7* mutants. (R and S) Accumulation of SQST-1::GFP aggregates in the muscle in *sta-2* mutants (R') is not suppressed by *dpy-10* inactivation (S). (A, J, N, and R) DIC images of the animals shown in A', J', N', and R', respectively. (T) Loss of function of *daf-3* suppresses accumulation of SQST-1::GFP aggregates in the muscle in *dpy-10; sta-2* mutants. (U–X) Quantification of the number of SQST-1::GFP aggregates in the indicated strains carrying the indicated transgene ($n = 5$ for each strain). Data are shown as mean \pm SEM; ***, $P < 0.001$. (Y) A model for the role of the *dpy-10* family genes in autophagy regulation. Cuticle damage, caused by depletion of cuticle annular furrow collagens, is sensed by cilia and further transduced by secretion of the TGF β ligand DAF-7 from neurons. DAF-3 functions cell autonomously in the hypodermis, intestine, and muscle to modulate autophagy activity. AAK-2, STA-2, and PMK-1 act differentially in different tissues for autophagy activation. Scale bars: A and B, 100 μ m; E–T, 20 μ m.

acids from DPY-10. *bpl242* contains a glycine-to-arginine mutation at amino acid 126 in DPY-2.

RNAi in *C. elegans*

RNAi bacterial clones were cultured on nematode growth medium agar plates containing 1 mM IPTG. L1 larval animals were plated onto RNAi feeding plates, and the F1 progeny were examined for the corresponding phenotype. For RNAi injection, single-strand RNA was synthesized by Large Scale RNA Production System T7 and SP6 kits (Promega, P1300 and P1280). Single-strand RNAs were then mixed and injected into animals. The F1 progeny were analyzed.

Generation of transgenic animals

To generate tissue-specific *daf-3* expression constructs, the *y37al.b5* promoter (2.9 kb; also known as the *hyp7* promoter), *hlh-1* promoter (2.9 kb), *ges-1* promoter (3.3 kb), and *gpa-4* promoter (3.0 kb) were amplified by PCR from genomic DNA. The PCR-amplified promoter region was inserted between the SphI and XmaI sites of the pPD49.26 vector, and the full-length *daf-3* cDNA was then inserted between the KpnI and SacI sites. The constructs were confirmed by sequencing. The constructs were injected into animals at a concentration of 20 ng/μl with a co-marker, *Pord-1::rfp* (50–100 ng/μl). At least three independent transgenic lines were analyzed for each rescue experiment.

To construct *Pgpa-4::daf-7*, 3.0-kb *gpa-4* promoter was cloned into pPD49.26 at the PstI/XmaI sites, and 1.9-kb *daf-7* genomic DNA was then inserted at the KpnI/SacI sites. To generate *Pdaf-7::GFP* reporter, 3.0-kb *daf-7* promoter was cloned into pPD49.26-GFP at the PstI site.

Real-time RT-PCR

Total RNA was extracted from synchronized animals using Trizol reagent. Quantitative PCR reactions were performed using UltraSYBR Mixture RT-PCR kits (CWBIO, CW2602M) and a PCR biosystems QuantStudio 7 Flex. Three independent experiments were performed. The results were analyzed with GraphPad Prism 5.

Quantification and statistical analysis

For quantification of the number of SQST-1::GFP aggregates, images were captured with a microscope (Zeiss M2) at 400× magnification. Images were captured at similar regions in the animals at the same developmental stage using the same exposure time. The number of SQST-1::GFP aggregates was quantified using ZEN lite 2011 and analyzed with GraphPad Prism 5. Five animals for each strain were used for quantification. For measurement of the fluorescence intensity of GFP::LGG-1 puncta, images were acquired at 630× magnification using a Zeiss LSM880 microscope. For quantification of the fluorescence intensity of *Paak-2::AAK-2::Tomato*, *Pnlp-29::GFP*, and *Pgpdh-1::GFP*, images were acquired at 100× magnification using a Zeiss M2 microscope. Images were quantified using ImageJ (National Institutes of Health) and analyzed with GraphPad Prism 5. At least five animals were analyzed. Immunoblotting results are representative of three independent experiments. The intensity of Western blot signals was quantified using

ImageJ. Statistical comparisons were made using the two-tailed unpaired Student's *t* test, and the results are shown as mean ± SEM; ns, no significant difference, *P* > 0.05; *, *P* < 0.05; **, *P* < 0.01; ***, *P* < 0.001.

Online supplemental material

Fig. S1 shows elevated autophagy activity in *dpy-10* mutants. Fig. S2 shows the requirement of functional cilia in systemic autophagy induction in *dpy-10* mutants. Fig. S3 shows the requirement of TGFβ signaling in systemic autophagy activation in *dpy-10* mutants. Functional cilia, dauer TGFβ signaling, and AMPK/AAK-2 are not involved in the innate immune response and hypertonic stress response in *dpy-10* mutants.

Acknowledgments

We are grateful to Dr. Isabel Hanson for editing work and Dr. Malene Hansen (Sanford Burnham Prebys Medical Discovery Institute, La Jolla, CA) for the AAK-2(aal-321)::Tomato strain.

This work was supported by the following grants to H. Zhang: Beijing Municipal Science and Technology Commission (Z181100001318003), Chinese Ministry of Science and Technology 017YFA0503401, National Natural Science Foundation of China (31421002, 31561143001, 31630048, and 31790403), Strategic Priority Research Program of the Chinese Academy of Sciences (grant XDB19000000), and Key Research Program of Frontier Sciences, Chinese Academy of Sciences (grant QYZDY-SSW-SMC006).

The authors declare no competing financial interests.

Author contributions: H. Zhang designed the experiments. Y.J. Zhang and L.X. Qi performed the experiments. H. Zhang wrote the manuscript.

Submitted: 26 July 2019

Revised: 16 September 2019

Accepted: 19 September 2019

References

- Dierking, K., J. Polanowska, S. Omi, I. Engelmann, M. Gut, F. Lembo, J.J. Ewbank, and N. Pujol. 2011. Unusual regulation of a STAT protein by an SLC6 family transporter in *C. elegans* epidermal innate immunity. *Cell Host Microbe*. 9:425–435. <https://doi.org/10.1016/j.chom.2011.04.011>
- Feng, Y., D. He, Z. Yao, and D.J. Klionsky. 2014. The machinery of macroautophagy. *Cell Res*. 24:24–41. <https://doi.org/10.1038/cr.2013.168>
- Fenouille, N., A.C. Nascimbeni, J. Botti-Millet, N. Dupont, E. Morel, and P. Codogno. 2017. To be or not to be cell autonomous? Autophagy says both. *Essays Biochem*. 61:649–661. <https://doi.org/10.1042/EBC20170025>
- Guo, B., Q. Liang, L. Li, Z. Hu, F. Wu, P. Zhang, Y. Ma, B. Zhao, A.L. Kovács, Z. Zhang, et al. 2014. O-GlcNAc-modification of SNAP-29 regulates autophagosome maturation. *Nat. Cell Biol*. 16:1215–1226. <https://doi.org/10.1038/ncb3066>
- Hu, P.J. 2007. Dauer (May 21, 2007). *WormBook*. <https://doi.org/10.1895/wormbook.1.144.1>
- Inglis, P.N., G. Ou, M.R. Leroux, and J.M. Scholey. 2007. The sensory cilia of *Caenorhabditis elegans* (November 22, 2006). *WormBook*. <https://doi.org/10.1895/wormbook.1.126.1>
- Kanasaki, K., E. Kawakita, and D. Koya. 2019. Relevance of autophagy induction by gastrointestinal hormones: focus on the incretin-based drug target and glucagon. *Front. Pharmacol*. 10:476. <https://doi.org/10.3389/fphar.2019.00476>
- Kang, C., and L. Avery. 2009. Systemic regulation of starvation response in *Caenorhabditis elegans*. *Genes Dev*. 23:12–17. <https://doi.org/10.1101/gad.1723409>

- Katheder, N.S., R. Khezri, F. O'Farrell, S.W. Schultz, A. Jain, M.M. Rahman, K.O. Schink, T.A. Theodossiou, T. Johansen, G. Juhász, et al. 2017. Microenvironmental autophagy promotes tumour growth. *Nature*. 541: 417–420. <https://doi.org/10.1038/nature20815>
- Kaushik, S., J.A. Rodriguez-Navarro, E. Arias, R. Kiffin, S. Sahu, G.J. Schwartz, A.M. Cuervo, and R. Singh. 2011. Autophagy in hypothalamic AgRP neurons regulates food intake and energy balance. *Cell Metab.* 14: 173–183. <https://doi.org/10.1016/j.cmet.2011.06.008>
- Lamitina, T., C.G. Huang, and K. Strange. 2006. Genome-wide RNAi screening identifies protein damage as a regulator of osmoprotective gene expression. *Proc. Natl. Acad. Sci. USA*. 103:12173–12178. <https://doi.org/10.1073/pnas.0602987103>
- Li, C., and K. Kim. 2008. Neuropeptides (February 5, 2008). *WormBook*. <https://doi.org/10.1895/wormbook.1.142.1>
- Li, W., S.G. Kennedy, and G. Ruvkun. 2003. daf-28 encodes a C. elegans insulin superfamily member that is regulated by environmental cues and acts in the DAF-2 signaling pathway. *Genes Dev.* 17:844–858. <https://doi.org/10.1101/gad.1066503>
- Lin, L., F.S.L.M. Rodrigues, C. Kary, A. Contet, M. Logan, R.H.G. Baxter, W. Wood, and E.H. Baehrecke. 2017. Complement-Related Regulates Autophagy in Neighboring Cells. *Cell*. 170:158–171.e8. <https://doi.org/10.1016/j.cell.2017.06.018>
- Lin, L., P. Yang, X. Huang, H. Zhang, Q. Lu, and H. Zhang. 2013. The scaffold protein EPG-7 links cargo-receptor complexes with the autophagic assembly machinery. *J. Cell Biol.* 201:113–129. <https://doi.org/10.1083/jcb.201209098>
- McMahon, L., J.M. Muriel, B. Roberts, M. Quinn, and I.L. Johnstone. 2003. Two sets of interacting collagens form functionally distinct substructures within a *Caenorhabditis elegans* extracellular matrix. *Mol. Biol. Cell*. 14:1366–1378. <https://doi.org/10.1091/mbc.e02-08-0479>
- McPhee, C.K., M.A. Logan, M.R. Freeman, and E.H. Baehrecke. 2010. Activation of autophagy during cell death requires the engulfment receptor Draper. *Nature*. 465:1093–1096. <https://doi.org/10.1038/nature09127>
- Meisel, J.D., O. Panda, P. Mahanti, F.C. Schroeder, and D.H. Kim. 2014. Chemosensation of bacterial secondary metabolites modulates neuroendocrine signaling and behavior of *C. elegans*. *Cell*. 159:267–280. <https://doi.org/10.1016/j.cell.2014.09.011>
- Meléndez, A., Z. Tallóczy, M. Seaman, E.L. Eskelinen, D.H. Hall, and B. Levine. 2003. Autophagy genes are essential for dauer development and life-span extension in *C. elegans*. *Science*. 301:1387–1391. <https://doi.org/10.1126/science.1087782>
- Mihaylova, M.M., and R.J. Shaw. 2011. The AMPK signalling pathway coordinates cell growth, autophagy and metabolism. *Nat. Cell Biol.* 13: 1016–1023. <https://doi.org/10.1038/ncb2329>
- Mizushima, N., and M. Komatsu. 2011. Autophagy: renovation of cells and tissues. *Cell*. 147:728–741. <https://doi.org/10.1016/j.cell.2011.10.026>
- Mizushima, N., T. Yoshimori, and Y. Ohsumi. 2011. The role of Atg proteins in autophagosome formation. *Annu. Rev. Cell Dev. Biol.* 27:107–132. <https://doi.org/10.1146/annurev-cellbio-092910-154005>
- Page, A.P., and I.L. Johnstone. 2007. The cuticle (January 23, 2007). *WormBook*. <https://doi.org/10.1895/wormbook.1.138.1>
- Perkins, L.A., E.M. Hedgecock, J.N. Thomson, and J.G. Culotti. 1986. Mutant sensory cilia in the nematode *Caenorhabditis elegans*. *Dev. Biol.* 117: 456–487. [https://doi.org/10.1016/0012-1606\(86\)90314-3](https://doi.org/10.1016/0012-1606(86)90314-3)
- Pujol, N., S. Cypowyj, K. Ziegler, A. Millet, A. Astrain, A. Goncharov, Y. Jin, A.D. Chisholm, and J.J. Ewbank. 2008a. Distinct innate immune responses to infection and wounding in the *C. elegans* epidermis. *Curr. Biol.* 18:481–489. <https://doi.org/10.1016/j.cub.2008.02.079>
- Pujol, N., O. Zugasti, D. Wong, C. Couillault, C.L. Kurz, H. Schulenburg, and J.J. Ewbank. 2008b. Anti-fungal innate immunity in *C. elegans* is enhanced by evolutionary diversification of antimicrobial peptides. *PLoS Pathog.* 4:e1000105. <https://doi.org/10.1371/journal.ppat.1000105>
- Richmond, J.E., W.S. Davis, and E.M. Jorgensen. 1999. UNC-13 is required for synaptic vesicle fusion in *C. elegans*. *Nat. Neurosci.* 2:959–964. <https://doi.org/10.1038/14755>
- Russell, R.C., H.X. Yuan, and K.L. Guan. 2014. Autophagy regulation by nutrient signaling. *Cell Res.* 24:42–57. <https://doi.org/10.1038/cr.2013.166>
- Tian, Y., Z. Li, W. Hu, H. Ren, E. Tian, Y. Zhao, Q. Lu, X. Huang, P. Yang, X. Li, et al. 2010. *C. elegans* screen identifies autophagy genes specific to multicellular organisms. *Cell*. 141:1042–1055. <https://doi.org/10.1016/j.cell.2010.04.034>
- Ulgherait, M., A. Rana, M. Rera, J. Graniel, and D.W. Walker. 2014. AMPK modulates tissue and organismal aging in a non-cell-autonomous manner. *Cell Reports*. 8:1767–1780. <https://doi.org/10.1016/j.celrep.2014.08.006>
- Wang, Z., G. Miao, X. Xue, X. Guo, C. Yuan, Z. Wang, G. Zhang, Y. Chen, D. Feng, J. Hu, and H. Zhang. 2016. The Vici syndrome protein EPG5 is a Rab7 effector that determines the fusion specificity of autophagosomes with late endosomes/lysosomes. *Mol. Cell*. 63:781–795. <https://doi.org/10.1016/j.molcel.2016.08.021>
- Wheeler, J.M., and J.H. Thomas. 2006. Identification of a novel gene family involved in osmotic stress response in *Caenorhabditis elegans*. *Genetics*. 174:1327–1336. <https://doi.org/10.1534/genetics.106.059089>
- Yang, P., and H. Zhang. 2014. You are what you eat: multifaceted functions of autophagy during *C. elegans* development. *Cell Res.* 24:80–91. <https://doi.org/10.1038/cr.2013.154>
- Zhang, H., J.T. Chang, B. Guo, M. Hansen, K. Jia, A.L. Kovács, C. Kumsta, L.R. Lapierre, R. Legouis, L. Lin, et al. 2015a. Guidelines for monitoring autophagy in *Caenorhabditis elegans*. *Autophagy*. 11:9–27.
- Zhang, Y., W. Li, L. Li, Y. Li, R. Fu, Y. Zhu, J. Li, Y. Zhou, S. Xiong, and H. Zhang. 2015b. Structural damage in the *C. elegans* epidermis causes release of STA-2 and induction of an innate immune response. *Immunity*. 42:309–320. <https://doi.org/10.1016/j.immuni.2015.01.014>
- Zhao, Y.G., and H. Zhang. 2018. Formation and maturation of autophagosomes in higher eukaryotes: a social network. *Curr. Opin. Cell Biol.* 53: 29–36. <https://doi.org/10.1016/j.ceb.2018.04.003>